

Using Ca-Fe layered double hydroxide transformation to optimise phosphate removal from waste waters

Muayad Al Jaber^a, Martine Mallet^a, H. Chris Greenwell^b, Mustapha Abdelmoula^a and Christian Ruby^{a,*}

^aLaboratoire de Chimie Physique et Microbiologie pour les Matériaux et l'Environnement, LCPME UMR 7564 CNRS-Université de Lorraine, 405 rue de Vandoeuvre 54600 Villers-lès-Nancy, France.

^bDepartment of Earth Sciences, Durham University, South Road, Durham DH1 3LE, UK.

* Corresponding author: Christian.ruby@univ-lorraine.fr

Postal address: LCPME, 405 rue de Vandoeuvre 54600 Villers-lès-Nancy, France.

Abstract

Single phase Ca-Fe layered double hydroxide (LDH) minerals containing Cl⁻ species in the interlayer was synthesised by coprecipitation with a Ca^{II}: Fe^{III} ratio of 2 : 1. In both phosphate (PO₄) free water and at low aqueous PO₄ concentration, the LDH was fully transformed into a mixture of a “ferrihydrite-like” material, calcite and soluble calcium species. Mössbauer spectroscopy and transmission electron microscopy showed that phosphate was removed by the “ferrihydrite like” phase that contained a significant quantity of Ca. At high phosphate concentration the Ca species released from the LDH precipitated to form hydroxyapatite leading to a maximal removal capacity of ~ 130 mg P-PO₄ g⁻¹. The Ca-Fe LDH was deposited onto a pozzolana volcanic rock in order to perform a column experiment under hydrodynamic conditions for 70 days. A high removal capacity was observed, a q_B of ~ 4 mg P-

22 $\text{PO}_4 \text{ g}^{-1}$ was measured at the breakthrough of the column, however the pH in the outflow was measured
23 to be higher than 11. Such an increase was due to the very high solubility of the Ca-Fe LDH.

24 **Keywords** : LDH; Iron; Water treatment; Adsorption; Precipitation; Hydroxyapatite

25

26 **1. Introduction**

27 Protection and monitoring of water resources are among the major issues of the twenty-first century
28 due to population growth, rapid industrialization and intensification of agriculture. Among the various
29 pollutants that threaten water quality, orthophosphate species ($\text{H}_{3-x}\text{PO}_4^{x-}$ subsequently named PO_4)
30 are of utmost importance since the excess of PO_4 is mainly responsible for the phenomena of water
31 eutrophication. Eutrophication leads to strong perturbation of biodiversity and important economic
32 losses, *e.g.* closing of fisheries and groundwater production wells. As an example, an annual cost of €
33 1.75 million was estimated for the freshwater of the USA alone (Dodds et al., 2009). One of the causes
34 of excess PO_4 in water is the lack of adequate PO_4 treatment and monitoring in waste water treatment
35 plants (WWTP), in particular in ecologically more sensitive rural areas. For economic reasons classical
36 waste water treatments that needs costly infrastructure are often not performed, *e.g.* installations
37 using the activated sludge process in either low population, remote or developing areas. Therefore,
38 WWTP using passive water treatment technologies such as reed bed filters are often preferred. Natural
39 materials such as hydroxyapatite, or industrial waste such as steel slag, were used at the pilot scale to
40 remove phosphate from wastewater (Vohla et al., 2011). If such materials are intended to be used in
41 horizontal filters, the dimensioning of the reactors depends on numerous factors such as: (i) the
42 number of population equivalent (PE) releasing wastewater, (ii) the quantity of P- PO_4 released by 1 PE
43 per day {typically in the range of ~ 1 to ~ 3 g
44 P- PO_4 PE⁻¹ (Henze and Comeau, 2008)}, (iii) the PO_4 removal capacity ($\text{mg P-PO}_4 \text{ g}^{-1}$) of the Filtration
45 Material (FM) under hydrodynamic flow and (iv) the duration of the water treatment until the material
46 is saturated with PO_4 . As an example, a volume of $\sim 0.8 \text{ m}^3$ of FM per PE was estimated to be necessary

47 for a 4 years treatment if ferrihydrite coated pozzolana was used as a FM (Ruby et al., 2016). Such a
48 volume of FM corresponds also to a surface $\sim 2 \text{ m}^2$ per PE for a horizontal filter with a depth of 0.5 m.
49 Therefore, passive water treatments are generally extensive and need relatively high amount of FM
50 that occupy a relatively large surface. As explained by Vohla (Vohla et al., 2011), large-scale and long-
51 term (typically 5 years) experiments are absolutely necessary for evaluating accurately the optimal
52 quantity and lifetime of the FM in such filters. A possibility for reducing the size of the filtration reactors
53 is to synthesize FM characterized by a much higher PO_4 removal capacity. For this purpose, Layered
54 Double Hydroxides (LDH) are particularly interesting materials. They constitute of stacking of
55 hydroxide layers containing divalent M^{II} and trivalent M^{III} cations. The positive charge of the cationic
56 sheets is counterbalanced by the presence of anions $\text{A}^{\text{n-}}$ and water molecules present in the interlayer.
57 LDH obey the general chemical formula $[\text{M}^{\text{II}}_{(1-x)}\text{M}^{\text{III}}_x(\text{OH})_2]^{x+} [x/n \text{ A}^{\text{n-}} \text{ m H}_2\text{O}]^{x-}$ where x represents both
58 the charge of the layers and the M^{III} molar fraction. The values of x depend on the nature of the M^{II}
59 and M^{III} cations and vary in a range from ~ 0.1 to 0.33 (Forano et al., 2013). LDH can remove PO_4 by
60 several mechanisms such as adsorption, anionic exchange or dissolution-precipitation (Baliarsingh et
61 al., 2013). The Theoretical PO_4 Removal Capacity of an LDH (TPRC in mg g^{-1}) by anionic exchange
62 depends on the M^{III} molar fraction (x), the charge (n) of the replacing anions and on the LDH molar
63 mass. As discussed later in this work, the maximal TPRC of Ca-Fe LDH will be estimated to be as high
64 as $\sim 110 \text{ mg P-PO}_4 \text{ g}^{-1}$, a value much higher than the removal capacity reported in homogeneous batch
65 dispersion for other minerals such as ferrihydrite $\{\sim 26 \text{ mg P-PO}_4 \text{ g}^{-1}$ (Ruby et al., 2016)}, steel slag (up
66 to $\sim 2.4 \text{ mg PO}_4 \text{ g}^{-1}$ (Barca et al., 2012) or hydroxyapatite ($0.3 \text{ mg P-PO}_4 \text{ g}^{-1}$ (Bellier et al., 2006)). Maximal
67 phosphate removal capacities $\{q_e^{(\text{Max})}\}$ of the same order of magnitude than the TPRC were in fact
68 reported by different authors studying the interaction of Ca based LDH such as Ca-Al LDH (Bekele et
69 al., 2019; Jia et al., 2016; Oladoja et al., 2014; Qian et al., 2012), *i.e.* hydrocalumite, Ca-Mg-Al LDH
70 (Ashekuzzaman et al., 2014) and Ca-Fe LDH (Ashekuzzaman et al., 2014; Tsuji and Fujii, 2014).
71 However, for both Ca-Al LDH and Ca-Fe LDH, the reported values of $q_e^{(\text{Max})}$ varied in a relatively broad
72 range between ~ 46 and $\sim 179 \text{ mg P-PO}_4 \text{ g}^{-1}$ depending on experimental conditions, *e.g.* LDH synthesis

73 procedure, phosphate concentration, adsorbent dose and pH. Several authors reported the
74 mineralogical transformation of the LDH into a calcium phosphate phase such as hydroxyapatite (Qian
75 et al., 2012; Tsuji and Fujii, 2014) or brushite (Bekele et al., 2019; Jia et al., 2016), in particular for high
76 PO_4 concentrations ($150 \text{ mg L}^{-1} \leq [\text{PO}_4] \leq 1500 \text{ mg L}^{-1}$). At lower PO_4 concentrations, a significant
77 decrease of intensity and a general broadening of the LDH X-ray diffraction (XRD) peaks were observed
78 (Ashekuzzaman et al., 2014; Oladoja et al., 2014). The synthesis of Ca-Fe LDH was reported to lead to
79 a higher degree of crystallinity in comparison to Mg-Al LDH, i.e. hydrotalcite (Tsuji and Fujii, 2014).
80 However, the concomitant formation of secondary phases supposed to be $\text{Ca}(\text{OH})_2$, " $\text{Fe}(\text{OH})_3$ " and
81 CaCO_3 was noted when varying the Ca : Fe ratio between 0.75 and 3. In a recent study we
82 demonstrated that almost single phase Ca-Fe LDH can only be synthesized for a Ca : Fe ratio of 2 : 1,
83 with a higher ratio leading to the formation of either $\text{Ca}(\text{OH})_2$ or CaCO_3 depending on the synthesis
84 procedure (Al-Jaberi et al., 2015).

85 The first goal of this study was to determine as precisely as possible the mineralogical transformation
86 of single phase Ca-Fe LDH in the presence of PO_4 solutions of varying concentrations. The behavior
87 observed at lower PO_4 concentration ($< \sim 100 \text{ mg L}^{-1}$) will be particularly relevant for application in
88 waste water treatment where the concentration of PO_4 is often between ~ 10 and $\sim 60 \text{ mg L}^{-1}$ (Ruby
89 et al., 2016). Moreover, we recently developed a new method of synthesis allowing the deposition of
90 a high amount of ferrihydrite onto a pozzolana support (Ruby et al., 2015). Such a method of synthesis
91 was adapted here to synthesize pozzolana coated with Ca-Fe LDH (Ca-Fe LDH-Pz). The second goal of
92 this study was to study the PO_4 removal by Ca-Fe LDH-Pz under hydrodynamic conditions. Such an
93 experiment is of utmost importance if the material is finally intended to be used for horizontal, or
94 vertical, filters in the field.

95

96

97 **2. Experimental**

98 2.1 Chemical Products

99 Calcium chloride dihydrate ($\text{CaCl}_2 \cdot 2\text{H}_2\text{O}$), iron (III) chloride hexahydrate ($\text{FeCl}_3 \cdot 6\text{H}_2\text{O}$) and sodium
100 hydrogenophosphate dehydrate ($\text{NaH}_2\text{PO}_4 \cdot 2\text{H}_2\text{O}$) were purchased from Sigma-Aldrich with a purity
101 greater than 99%. Sodium hydroxide was procured from Carlo Erba with purity greater than 99%. The
102 pozzolana (Pz) was supplied by "Pouzzolanes des Domes" (Saint-Ours-les-Roches, France) and was
103 characterized by a grain size ranging from 1 to 3 mm. As already described previously (Ruby et al.,
104 2015), pozzolana is a porous material comprised of a mixture of labradorite ($\text{Na,Ca}(\text{Al,Si})_4\text{O}_8$, diopside
105 $\text{CaMgSi}_2\text{O}_6$, forsterite Mg_2SiO_4 and hematite $\alpha\text{-Fe}_2\text{O}_3$.

106 2.2 Materials synthesis

107 *2.2.1 Synthesis of Ca-Fe LDH*

108 The method of synthesis of the Ca-Fe LDH was optimized in a previous study (Al-Jaberi et al., 2015).
109 Briefly, a first solution (A) was prepared by dissolving 66.7 mmol of Ca(II) and 33.3 mmol of Fe(III) salts
110 ($\text{Ca(II)} : \text{Fe(III)} = 2 : 1$) into 300 mL of demineralized ultrapure water (18.2 M Ω). Solution A was
111 introduced progressively with the help of a peristaltic pump (total time of 150 min.) into a 300 mL
112 solution B containing 200 mmol of NaOH ($\text{OH}^- / \{\text{Ca(II)} + \text{Fe(II)}\} = 2$) to precipitate the LDH product. At
113 the end of the experiment the pH was between 11.4 and 11.8. The LDH dispersion was filtered under
114 suction through a Buchner funnel using 22 μm pore size Millipore[®] paper filter. All the filtered samples
115 were thoroughly washed with distilled water and cold ethanol, dried at room temperature and ground
116 in a mortar to obtain a fine powder.

117 *2.2.2 Synthesis of Ca-Fe LDH coated pozzolana*

118 A mass of 20 g of Ca-Fe powder was mixed with 100 g of Pz in a dry state in a 500 mL plastic wide
119 necked bottle. The mixture was shaken during 12 h using a Reax 20/8 overhead shaker (Heidolph
120 Instruments GmbH & Co.K.G, Schwabach, Germany) with a rotation speed of 16 rpm. The LDH coated
121 Pz was subjected to the separation of free particles with a 40 mesh sieve. The quantity of LDH
122 deposited onto Pz was estimated to be 14.2 ± 0.4 g% by comparing the weight of the material before
123 and after coating.

124

125 2.3 Characterization of the samples

126 2.3.1 X-Ray Diffraction (XRD).

127 The crystal structure of the samples was studied by XRD using a Philips X'Pert pro MPD diffractometer
128 (CuK α radiation $\lambda = 1.5418 \text{ \AA}$). Patterns were collected with a step size of 0.03342° and a rate of 87.63
129 s per step.

130 2.3.2 Raman spectroscopy

131 Raman spectra were recorded in backscattering configuration by using a Horiba Jobin-Yvon T64000
132 spectrometer, equipped with an Ar²⁺ laser emitting at 514.53 nm in the range 100 to 4000 cm⁻¹. The
133 spectrum was setup with a 1800 groove mm⁻¹ diffraction grating, and a liquid N₂-cooled Charge
134 Coupled Device (CCD). The spectra resolution was set to 2 cm⁻¹ by selecting the entrance slit width.
135 The objective was x80 (0.95 of numerical aperture). The spectrometer was calibrated with the 520.7
136 cm⁻¹ line of a silicon wafer. The laser power was 200 mW.

137 2.3.3 Mössbauer spectrometry

138 Transmission Mössbauer spectrometry was performed using a ⁵⁷Co source to identify the iron
139 containing compounds. The filtered materials were transferred inside a cold head cryostat (Advanced
140 Research Systems) under an inert He atmosphere. Mössbauer spectra were recorded with a constant
141 acceleration spectrometer and a 512 multichannel analyser. The data were calibrated with a 25 μm
142 thick pure α -iron foil. Mössbauer spectra were fitted using the Recoil software. Shape lines were either
143 Lorentzian or Voigt profile, *i.e.* a convolution of a Gaussian distribution with a Lorentzian shape line.

144 2.3.4 Transmission Electron Microscopy (TEM).

145 The data were collected at the Competence Center for Electronics Microscopy and Microwaves
146 (Institut Jean Lamour UMR 7198 CNRS-Université de Lorraine) by using a JEOL JEM-ARM200F
147 apparatus. The sample was prepared by forming a dispersion of the dried solid product into ethanol.
148 One drop of the dispersion was laid on a copper grid for TEM analysis coupled with an Energy
149 Dispersive X-ray (EDX) analyzer.

150 *2.3.5 X-Ray Photoelectron spectroscopy (XPS)*

151 XPS spectra were recorded by using a Kratos Axis Ultra DLD (Manchester, UK) instrument. The spectra
152 were recorded at a normal (90°) angle between the surface of the sample and the direction of the
153 ejected electron. The acquisition of low-resolution spectra has been carried out with pass energy of
154 160 eV and steps of 1 eV and high resolution spectra with a pass energy of 20 eV and steps of 0.5 eV.
155 The analyzed area was 0.3x0.7 mm². The spectra were corrected for charging effects by using the C1s
156 contamination peak situated at 284.6 eV.

157 *2.3.6 Inductive Coupled Plasma Atomic Emission Spectroscopy (ICP-AES)*

158 Dissolved phosphate, calcium and iron species concentrations were measured by ICP-AES using a Jobin
159 Yvon-ULTIMA apparatus. The solutions were mixed into HNO₃ solutions to avoid the presence of trace
160 solid particles before analysis.

161

162 *2.4 Chemical reactivity of Ca-Fe LDH with phosphate*

163 *2.4.1 Batch experiments*

164 Phosphate solutions with various concentrations were prepared by dissolving NaH₂PO₄·2H₂O into
165 ultrapure water. All experiments were conducted at room temperature with a 0.1 M NaCl supporting
166 electrolyte and a pH of 7. All the pH measurements were carried out with a digital pH meter (Almemo
167 model 2690) using a glass electrode (model PHER 112 SE). The pH of the solutions was adjusted
168 manually to the required values by diluted NaOH or HCl solutions. The volume of acid/alkali added for
169 pH adjustment never exceeded 1% of the total volume. The PO₄ removal kinetics was studied over 48
170 h by adding 1 g of LDH in 1 L of phosphate solution, with concentrations varying in between 20 and
171 1000 mg L⁻¹ (0.21 to 10.53 mmol L⁻¹). The effect of the initial PO₄ concentrations (isotherm experiments)
172 was studied in another set of experiments where 0.1 g of LDH was introduced into 100 mL of PO₄
173 solution with an initial concentration varying between 20 and 2000 mg L⁻¹ for 24 h, this time period
174 having been previously determined from kinetics experiments as being sufficient for reaching quasi-
175 equilibrium conditions. At a selected time, 1 mL of the solution was withdrawn to determine PO₄

176 concentrations by ICP-AES and, as required, also other soluble species such as $\text{Ca}^{2+}_{\text{aq}}$ and $\text{Fe}^{3+}_{\text{aq}}$. Each
177 run was performed in duplicate and the results were averages of the two trials with reproducibility
178 within $\pm 5\%$.

179 *2.4.2 Column flow through experiments*

180 The column experiment was conducted in a Plexiglas[®] column with 3.7 cm internal diameter and 50
181 cm height. The column was loaded with 482 g of LDH coated Pz. The feed solution
182 ($[\text{PO}_4] = 100 \text{ mg L}^{-1}$) was continuously pumped in an up-flow mode from the reservoir through the
183 column at a flow rate of 1.1 mL min^{-1} using a peristaltic pump. The contact time was $\sim 5.5 \text{ h}$. Samples
184 were taken at regular time intervals in the outflow (2 sample per day) for 70 days for performing
185 chemical analyses with ICP-AES.

186

187 **3. Results**

188 3.1 Dissolution properties of Ca-Fe LDH in pure water

189 *3.1.1 Measurement of soluble Ca and Fe species*

190 Dried Ca-Fe LDH was introduced into demineralized water ($[\text{LDH}] = 1 \text{ g L}^{-1}$) under continuous stirring.
191 While soluble Fe concentration stayed below the detection limit of the ICP-AES due to the very low
192 solubility of Fe(III) species in alkaline solution, the soluble Ca concentration exhibited a strong increase
193 during the first 4 hours and reached a threshold value of 203 mg L^{-1} (Fig. 1). This value was in line with
194 the concentration of Ca measured in the solids of the pristine Ca-Fe LDH (300.5 mg g^{-1}) and the
195 hydrolysed product (100.6 mg g^{-1}). Therefore about 2/3 of the Ca species initially present in the solid
196 was released into solution and 1/3 was in a solid state. After a contact time of 48 hours the final pH of
197 water was 11.8.

198

199 *3.1.2 Mineralogical transformation of Ca-Fe LDH in pure water.*

200 The XRD patterns of the pristine LDH exhibited hydrocalumite-like structure (PDF 44-0445) (Fig. 2 a).

201 The pattern was indexed in a hexagonal lattice with a R-3 rhombohedral space group symmetry. A

202 d003-value of 7.77 Å was calculated in very good agreement with the value of 7.72 Å reported for Ca-
203 Fe-Cl LDH (Tsuji and Fujii, 2014). After a contact time with water of 24 h, the Ca-Fe LDH was completely
204 transformed as testified by the absence of LDH diffraction lines (Fig 2b). The resultant diffraction lines
205 were attributed to the formation of CaCO₃ meaning that a part of the Ca species present initially into
206 the LDH reacted with carbonate ions present in water under the strong alkaline conditions. Raman
207 spectroscopy was used to identify the solid phase containing the Fe^{III} species. Very similar features to
208 those recorded previously for two-line ferrihydrite were observed by Raman spectroscopy (Fig. 2c&d).
209 Indeed, the main bands of the ferrihydrite Raman spectra were reported to be situated at 223, 288
210 and 390 cm⁻¹ (Root et al., 2012). Two-line ferrihydrite also generally exhibited 2 low intensity XRD
211 diffraction peaks that were not clearly observed here (Fig. 2b), most probably due to the formation a
212 very disordered ferric structure in comparison to the well crystallised CaCO₃ compound. The full
213 dissolution of the Ca-Fe LDH was confirmed by XPS, and, indeed, the chloride ions intercalated in the
214 LDH were not detected with XPS anymore after 24 hours of contact time in water (Fig. SI-1).

215 3.2 Reactivity of Ca-Fe LDH with phosphate

216 3.2.1 Phosphate removal in batch experiments

217 The quantity of phosphate (PO₄) removed from water, q (mg P-PO₄ g⁻¹), was recorded (Fig. 3a) during
218 a period of 48 hours for a series of initial PO₄ concentrations ranging from 25 mg L⁻¹ to 1000 mg L⁻¹
219 ([LDH] = 1 g L⁻¹). The quantity of PO₄ removed from water increased rapidly during the first 4 hours and
220 reached a maximum value in between less than ~1 hour and ~ 8 hours for increasing PO₄
221 concentrations. As expected, the maximum value was achieved more quickly at low PO₄
222 concentrations. The maximum PO₄ removal obtained after 48 hours of contact time was plotted as a
223 function of the initial PO₄ concentrations (Fig 3b). The linear increase recorded in Zone A of the curve
224 corresponds to experiments where the removal rate R was equal or very close, to 100%. In this case
225 the concentration of PO₄ removed from the water was simply equal to the quantity of PO₄ introduced
226 into the solution. A maximum removal capacity, q_{Max} , of the Ca-Fe LDH is measured at higher PO₄

227 concentrations in zone B where R is lower than 100%. The value q_{Max} is close to $130 \text{ mg P-PO}_4 \text{ g}^{-1}$ for
228 the highest initial PO_4 concentration of 1000 mg L^{-1} and is relatively high in comparison to those
229 reported for Ca-Fe LDH, *i.e.* in between ~ 46 and $\sim 91 \text{ mg P-PO}_4 \text{ g}^{-1}$ (Table 1). The value of q_{Max} is also
230 significantly higher than the adsorption capacity of ferrihydrite ($\sim 20 \text{ mg PO}_4 \text{ g}^{-1} < q_{\text{Max}} < \sim 33 \text{ mg P-PO}_4$
231 g^{-1} in the pH range between 9 and 4, respectively). Note that ferrihydrite with a Surface Specific Area
232 (SSA) of $\sim 300 \text{ m}^2 \text{ g}^{-1}$ was reported to be the best PO_4 adsorbent of the iron oxide mineral family (Ruby
233 et al., 2016). This comparison with ferrihydrite suggests that Ca-Fe LDH interacted with PO_4 *via* another
234 mechanism than a simple adsorption process allowing the removal of a much higher quantity of PO_4 .

235 3.2.2 Mineralogical transformation of LDH in contact with PO_4

236 The solid products obtained after 48 hours of contact of the LDH with various PO_4 solutions were
237 analysed with XRD (Fig. 4). At a low PO_4 concentration (Fig. 4b), the XRD pattern obtained was quite
238 similar to the one observed previously in PO_4 -free water (Fig. 2b) and exhibited only the peaks of
239 CaCO_3 . For increasing PO_4 concentrations, new broad diffraction peaks appeared and sharpened
240 progressively at higher PO_4 concentrations (Fig 4c). These new peaks were attributed to the formation
241 of hydroxyapatite (HA) $\{\text{Ca}_5(\text{PO}_4)_3\text{OH}$, PDF 41-0490}. The progressive disappearance of the CaCO_3 XRD
242 peaks was concomitant with the progressive appearance of the HA XRD peaks (Fig. 4b-d). The kinetics
243 of transformation of the LDH as function of time was also studied for an initial PO_4 concentration of
244 600 mg L^{-1} (Fig. 5). In the very initial stages of the reaction, *e.g.* 10 min of reaction (Fig. 5b), the intensity
245 of the LDH peaks decreased and traces of CaCO_3 and HA were detected. The disappearance of the
246 diffraction peaks attributed to CaCO_3 and LDH occurred after 30 min and 4 h of reaction times,
247 respectively. Therefore, both CaCO_3 and the LDH were dissolved into soluble $\text{Ca}^{2+}_{\text{aq}}$ species that
248 partially precipitated with PO_4 to form HA. The dissolution of the LDH was much faster (30 min) in the
249 presence of a lower PO_4 concentration of (20 mg L^{-1}) and the final solid product was in this case CaCO_3
250 (Fig. SI2).

251 3.2.3 Correlation between the concentrations of soluble Ca and PO_4 species

252 The evolution of the PO₄ and Ca in solution after 48 h. of interaction between the LDH and PO₄ was
253 plotted as a function of the initial phosphate concentration (Fig. 6). In order to perform a mass balance
254 for the reactions, the concentrations were reported in mmol L⁻¹ (1 mmol L⁻¹ of PO₄ corresponds
255 approximatively to 100 mg L⁻¹ of PO₄). The soluble calcium concentration decreased almost linearly in
256 zone A ($0.2 \text{ mmol L}^{-1} \leq [\text{PO}_4]_0 \leq 2 \text{ mmol L}^{-1}$) when PO₄ anions were completely removed by the LDH. For
257 a critical PO₄ concentration of $\sim 2 \text{ mmol L}^{-1}$, the Ca²⁺_{aq} concentrations reached a value close to zero and
258 the PO₄ concentration began to increase. For [PO₄]₀ values higher than $\sim 2 \text{ mmol L}^{-1}$, the PO₄
259 concentration increased linearly with a slope of 1, meaning that an excess of PO₄ remained fully in
260 solution. The slope of the linear decrease of PO₄ concentration [$0.2 \text{ mmol L}^{-1} - 2 \text{ mmol L}^{-1}$] was
261 measured to be close to 5 : 2 (Ca : PO₄ = 2.5), a value significantly higher than the one expected if one
262 considers that phosphate was only removed by the precipitation of hydroxyapatite Ca₅(PO₄)₃OH (Ca :
263 PO₄ = 1.67). This result suggests that PO₄ was removed from water by another mechanism, or a
264 combination of mechanisms.

265

266 *3.2.4 Complementary analysis of the solid products obtained at low phosphate concentrations*

267 The XRD patterns obtained after the interaction of the LDH with PO₄ at low concentration did not
268 clearly exhibit the diffraction pattern of HA (Fig. 4 b-c), and therefore further investigations were
269 performed with TEM and Mössbauer spectroscopy. The products of transformation of the LDH with
270 [PO₄]₀ = 20 mg L⁻¹ consisted of CaCO₃ crystals mixed with an agglomeration of nanocrystals (Fig. 7).
271 Chemical analysis with EDX of the nanocrystals revealed the presence of O, Fe, Ca and P atoms
272 (Table 2). P atoms were not detected on CaCO₃ crystals (spot C & F) showing that calcite was inactive
273 for PO₄ removal. The chemical composition of the agglomerated nanocrystal was relatively
274 heterogeneous: calcium rich zones were detected in some areas (spots A, B, D & G) while iron rich
275 zones were detected in other areas (spots H & E). These nanocrystals containing Fe^{III} species were
276 assigned to the presence of a ferric paramagnetic doublet when probed with Mössbauer spectroscopy
277 at 77 K (Fig. 8a). The magnetic transition occurred at a temperature situated around 35 K (Fig. 8b) and

278 the Mössbauer spectra recorded at 14 K was essentially constituted of a distribution of very broad
279 sextets. A broad ferric doublet D_1 (RA of 10%) was added to obtained a good fit of the central part of
280 the spectrum (Table 3). The very broad range of the hyperfine field measured for the sextet's
281 distribution was situated in between 133 and 453 kOe such as those arising from superparamagnetism.
282 This observation was in agreement with the TEM data previously shown (Fig. 7), corresponding to the
283 formation of chemically heterogeneous nanocrystals containing Fe(III) and Ca(II) species.

284 *3.2.5 Column flow through experiments*

285 The potential of Ca-Fe LDH coated pozzolana for removing PO_4 was evaluated under hydrodynamic
286 conditions. The quantity of PO_4 measured in the outflow of the column ($[PO_4] / [PO_4]_0$) and the pH were
287 recorded as a function of V / V_p (Fig 9), where $[PO_4]_0$ is the concentration of phosphate in the inflow =
288 (100 mg L^{-1}), V is the total volume occupied by the filtration material and V_p the porous volume. The
289 pH in the outflow increased very rapidly from 4.6 to 11.3, in agreement with the LDH dissolution
290 process observed previously in homogeneous batch experiments. In the first step, the pH decreased
291 only very slowly and, in a second step, a sharp decrease was observed after 43 days of experiments
292 corresponding to a V / V_p value of 188. This value was also the critical volume corresponding to the
293 breakthrough of the column by the phosphate species: a sharp increase of the $[PO_4] / [PO_4]_0$ value was
294 observed and the concentration of PO_4 in the outflow was almost identical to the concentration of PO_4
295 in the inflow ($[PO_4] / [PO_4]_0 \sim 1$) after 70 days of experiment.

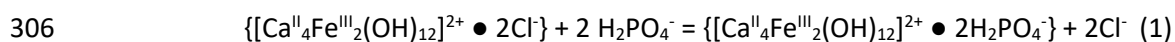
296 **4. Discussion**

297 4.1. Reactivity of Ca-Fe LDH with phosphate in batch experiments

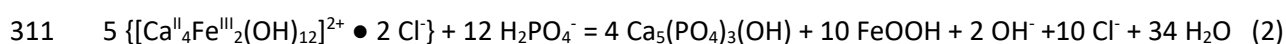
298 *4.1.1 Removal capacity at high phosphate concentration ($> 100 \text{ mg L}^{-1}$)*

299 Three types of reactions were considered in order to evaluate the corresponding phosphate removal
300 capacity. LDH are well known to be anion exchange materials and the question whether such a process
301 could be responsible for a phosphate removal capacity as high as $\sim 400 \text{ mg L}^{-1}$ arises. The removal

302 capacity by anionic exchange is strongly dependent on the speciation of the phosphate species (PO_4^{3-} ,
303 HPO_4^{2-} or H_2PO_4^-) present in the interlayer. Let us consider the intercalation of a monovalent H_2PO_4^-
304 that should lead to the maximal removal capacity *via* anionic exchange corresponding to the following
305 chemical reaction:



307 This reaction leads to a maximal removal capacity by anionic exchange of 113 mg P- $\text{PO}_4 \text{ g}^{-1}$ slightly
308 lower than the value measured in this study. According to the solid analysis, hydroxyapatite (HA) and
309 a ferric (hydr)oxide are the main products of transformation of the LDH. This corresponds to the
310 following chemical reaction:



312 This reaction leads to a removal capacity by dissolution-precipitation of 135 mg P- $\text{PO}_4 \text{ g}^{-1}$, which is in
313 better agreement with the value measured in this study. Note that the formation of a {HA, FePO_4 }
314 mixture would have led to an even higher removal capacity, of around 244 mg P- $\text{PO}_4 \text{ g}^{-1}$. Considering
315 reaction (2), one may hypothesize that at high phosphate concentration the removal of PO_4 was
316 essentially governed by the dissolution of Ca^{II} species present in the initial LDH reactant. A part of the
317 phosphate species may also be adsorbed on the ferric (hydr)oxide nanocrystals but the relative
318 proportion of this process in the overall phosphate removal was certainly lower. Indeed the PO_4
319 removal capacity of ferric (hydr)oxides is generally situated in a significantly lower range between 3
320 and 26 mg P- $\text{PO}_4 \text{ g}^{-1}$ (Mallet et al., 2013).

321 *4.1.2 Removal capacity at low phosphate concentration ($\leq 100 \text{ mg L}^{-1}$)*

322 The XRD patterns showed the progressive disappearance of HA when the phosphate concentration
323 decreased (Fig 5). This decrease was concomitant with a progressive decrease of the PO_4 removal
324 capacity. In the concentration range 25 - 100 mg L^{-1} , calcite CaCO_3 is formed rather than HA. Therefore,

325 a competitive association of Ca either with phosphate or carbonate was evidenced. This competition
326 was won either by phosphate, or by carbonate, at high and low PO₄ concentration, respectively.

327 TEM showed that calcite (CaCO₃) did not adsorb PO₄ species that were rather associated with a very
328 disordered solid phase containing both Ca^{II} and Fe^{III} species. Therefore, a significant proportion of the
329 Ca^{II} species initially present in the LDH phase did not participate to the PO₄ removal and are either
330 released as soluble species or present in CaCO₃. However, a minor part of the Ca species coexists with
331 Fe species in a solid phase resembling ferrihydrite. As previously described (Ruby et al., 2016) the co-
332 existence of Ca species and ferrihydrite led to a global increase of PO₄ removal in comparison to Ca
333 free ferrihydrite. Such a synergistic effect may explain the relatively high PO₄ removal observed even
334 at low PO₄ concentrations in this study, e.g. for an initial PO₄ concentration of 100 mg L⁻¹, the removal
335 capacity was not determined accurately since the removal rate was close to 100% and the Fe-Ca solid
336 surfaces are certainly under-saturated. However, the data showed that the removal capacity is at least
337 as high as 33 mg P-PO₄ g⁻¹, a value higher than those measured for Ca free iron oxides (Ruby et al.,
338 2016).

339 4.2 Reactivity of Ca-Fe LDH with phosphate in column experiment

340 The experiment performed in the column demonstrated that pozzolana (Pz) coated with Ca-Fe LDH
341 was particularly efficient for removing phosphate. Indeed, the experiment may be compared to
342 another set of column experiments performed recently using ferrihydrite (Fh) coated Pz (Ruby et al.,
343 2015; Ruby et al., 2016) where the experimental conditions were quite similar, *i.e.* identical dimensions
344 of the columns, [PO₄]= 100 mg L⁻¹ in the inflow, but with a contact time of ~ 8 h instead of ~ 5.5 h in
345 this study. The removal capacity measured here at the breakthrough for Ca-Fe LDH-Pz, *i.e.* $q_B \sim 4$ mg
346 P-PO₄ g⁻¹, was ~ 3.2 times higher than the value measured previously for Fh-Pz, *i.e.* $q_B \sim 1.3$ mg P-PO₄
347 g⁻¹. However, the pH values higher than 11 measured in the outflow represent a problem for an
348 eventual application for waste water treatment. Indeed, such pH values are significantly higher than
349 the usual discharge standards with pH values that should be situated in between 6 and 8.5. In order to

350 use Ca based LDH materials for such an application, a better control of the LDH dissolution properties
351 would be necessary. On one hand the dissolution of Ca is beneficial for PO₄ removal by precipitation,
352 but on the other hand the LDH dissolution leads also to the release of OH⁻ species by inducing an
353 increase of pH {see equation (2)}. According to the different reactions paths obtained in batch
354 experiments (Fig. 10), a significant proportion of the Ca species present in the LDH was not efficient
355 for PO₄ removal and was released in the aqueous medium. A decrease of the solubility of the LDH may
356 be obtained by introducing in the solid structure less soluble divalent species than Ca²⁺ such as Mg²⁺
357 (Ashekuzzaman et al., 2014). Tuning carefully the relative proportion of Ca^{II} and Mg^{II} in a ternary Ca^{II}-
358 Mg^{II}-Fe^{III} LDH system in order to control both the resulting pH at lower values and the amount of
359 dissolved Ca²⁺ and Mg²⁺ could be an interesting way to enhance the applicability of using these LDH
360 materials for PO₄ removal in wastewater. Less soluble LDH such as Mg-Al hydrotalcite or Mg-Fe
361 pyroaurite may also remove PO₄ by anionic exchange, a process that can be concomitant to adsorption
362 or precipitation of phosphate species. Natural hydroxyapatite or shell-sand was also studied for
363 removing PO₄ from wastewater; similarly a slow release of Ca²⁺ soluble species was suggested as an
364 efficient way for driving PO₄ removal by a surface precipitation process (Lyngsie et al., 2014; Molle et
365 al., 2005).

366

367 **5. Conclusion**

368 The interaction between Ca-Fe layered double hydroxide and phosphate species was studied both in
369 homogeneous dispersion and in a flow through column experiment. In phosphate free water, the LDH
370 was fully transformed into a mixture of a ferrihydrite-like Fe^{III}-Ca^{II} disordered solid phase, calcite CaCO₃
371 and soluble Ca²⁺_{aq} species. At high phosphate concentration ([PO₄] > 100 mg L⁻¹), Ca²⁺_{aq} species released
372 by the LDH precipitated as hydroxyapatite leading to the removal of a very high concentration of
373 phosphate (q_e ~ 130 mg P-PO₄ g⁻¹). At low phosphate concentration ([PO₄] ≤ 100 mg L⁻¹), phosphate is
374 most probably removed by adsorption on the ferrihydrite-like Fe^{III}-Ca^{II} compound. Pozzolana coated

375 with Ca-Fe LDH very efficiently removed phosphate from water under hydrodynamic conditions, the
376 breakthrough of the column occurring at least 3 times later in comparison to ferrihydrite coated
377 pozzolana (Ruby et al., 2015). However, the high solubility of the Ca-Fe LDH led also to a strong increase
378 of the pH (> 11) preventing any direct application of such a material for wastewater treatment. Future
379 work dedicated to the control of the slow release of $\text{Ca}^{2+}_{\text{aq}}$ and OH^- species leading to a partial
380 dissolution of the LDH may improve the overall performance of the material, *i.e.* a high PO_4 removal
381 capacity and concomitantly limited alkaline modification of the aqueous medium.

382 **Acknowledgment**

383 We would like to thank the Ministry of Higher Education and Scientific Research of Irak for the PhD
384 grant of Muayad Al-Jaberi. The authors would like also to thank Ghouti Medjahdi (CNRS, Institut Jean
385 Lamour, Université de Lorraine) for TEM experiments. Claire Genois and Manuel Dossot (LCPME,
386 Institut Jean Barriol, Université de Lorraine) are acknowledged for their help during ICP-AES and Raman
387 Spectroscopy experiments. Prof C. Ruby and Prof. C. Greenwell thank the Institute of Advanced Study
388 of Durham University for the collaborative opportunity. Indeed, C. Ruby was an IAS invited fellow in
389 Durham University from October to December 2017.

390

391 **References**

392 [1] Al-Jaberi, M., Naille, S., Dossot, M., Ruby, C., 2015. Interlayer interaction in Ca-Fe layered double
393 hydroxides intercalated with nitrate and chloride species, J. Mol. Struct. 1102, 253-260.

394 [2] Ashekuzzaman, S. M., Jiang, J.-Q., 2014. Study on the sorption-desorption-regeneration
395 performance of Ca-, Mg and CaMg-based layered double hydroxides for removing phosphate from
396 water, Chem. Eng. J. 246, 97-105.

- 397 [3] Baliarsingh, N.; Parida, K. M.; Pradhan, G. C., 2013. Influence of the nature and concentration of
398 precursor metal ions in the brucite layer of LDHs for phosphate adsorption - a review, RSC Adv. 3,
399 23865-23878.
- 400 [4] Barca, C., Gérente, C., Meyer, D., Chazarenc, F., Andrès, Y., 2012. Phosphate removal from synthetic
401 and real wastewater using steel slags produced in Europe, Water Res. 46, 2376-2384.
- 402 [5] Bekele, B., Lundehøj, L., Jensen, N. D., Nielsen, U. G., Forano, C., 2019. Sequestration of
403 orthophosphate by Ca₂Al-NO₃ layered double hydroxide – Insight into reactivity and mechanism, Appl.
404 Clay Sci. 176, 49-57.
- 405 [6] Bellier, N., Chazarenc, F., Comeau, Y., 2006. Phosphorus removal from wastewater by mineral
406 apatite, Water Res. 40, 2376-2384.
- 407 [7] Dodds, W. K., Bouska, W. W., Eitzmann, J. L., Pilger, T. J. , Pitts, K. L., Riley, A. J., Schloesser, J. T.
408 Thornbrugh, D. J., 2009. Eutrophication of U.S. Freshwaters: Analysis of Potential Economic Damages,
409 Environ. Sci. Technol 43 , 12-19.
- 410 [8] Forano, C., Costantino, U., Prévot, V., TaviotGueho, C., 2013. Chapter 14.1 - Layered Double
411 Hydroxides (LDH), Developments in Clay Science 5, 745-782.
- 412 [9] M. Henze, Y. Comeau, 2008. Wastewater characterization in M. Hence, M.C.M. van Loosdrecht,
413 G.A. Ekama, D. Brdjanovic (Eds.), Biological Wastewater Treatment: Principles, Design and Modelling,
414 IWA Publishing, London, pp 33-52.
- 415 [10] Jia, Y., Wang, H., Zhao, X., Liu, X., Wang, Y., Fan, Q., Zhou, J., 2016. Kinetics, isotherms and multiple
416 mechanisms of the removal for phosphate by Cl-hydrocalumite, Appl. Clay Sci. 129, 116-121.
- 417 [11] Lyngsie, G., Borggaard, O.K., Hansen, H. C. B., 2014. A three-step test of phosphate sorption
418 efficiency of potential agricultural drainage filter materials, Water Res. 51, 256-265.

419 [12] Mallet, M., Barthélémy, K., Ruby, C., Renard, A., Naille, S., 2013. Investigation of phosphate
420 adsorption onto ferrihydrite by X-ray Photoelectron Spectroscopy, *J. Colloid Interface Sci.* 407, 95-101.

421 [13] Molle, P., Liénard, A., Grasmick, A., Iwema, A., Kabbabi, A. 2005. Apatite as an interesting seed to
422 remove phosphorus from wastewater in constructed wetlands, *Water Sci. Technol.* 51, 193-203.

423 [14] Oladoja, N.A., Adelagun, R.O.A., Ololade, I.A., Anthony, E.T., Alfred, M.O., 2014. Synthesis of nano-
424 sized hydrocalumite from a Gastropod shell for aquasystem phosphate removal, *Sep. Purif. Technol.*
425 124, 186-194.

426 [15] Qian, G., Feng, L., Zhou, J. Z., Xu, Y., Liu, J., Zhang, J., Xu, Z. P., 2012. Solubility product (K_{sp})-
427 controlled removal of chromate and phosphate by hydrocalumite, *Chem. Eng. J.*, 181-182, 251-258.

428 [16] Rietra, R. P. J. J., Hiemstra, T., van Riemsdijk, W. H., 2001. Interaction between calcium and
429 phosphate adsorption on goethite, *Environ. Sci. Technol.*, 35, 3369-3374.

430 [17] Rout, K., Mohapatra, M., Anand, S., 2012. 2-Line ferrihydrite: synthesis, characterization and its
431 adsorption behavior for removal of Pb(II), Cd(II), Cu(II) and Zn(II) from aqueous solutions, *Dalton Trans.*
432 41, 3302-3312.

433 [18] Ruby, C., Barthélémy, K., Hanna, K., Mallet, M., Naille, S., 2015. Synthesis process and
434 hydrodynamic behavior of a new filtration material for passive wastewater dephosphatation, *Mater.*
435 *Des.* 86, 168-177.

436 [19] Ruby, C., Naille, S., Ona-Nguema, G., Morin, G., Mallet, M., Guerbois, D., Barthélémy, K., Etique,
437 M., Zegeye, A., Zhang, Y., Boumaïza, H., Al-Jaberi, M., Renard, A., Noël, V., Binda, P., Hanna, K., Despas,
438 C., Abdelmoula, M., Kukkadapu, R., Sarrias, J., Albignac, M., Rocklin, P., Nauleau, F., Hyvrard N., Génin,
439 J.-M., 2016. Use of Ferrihydrite-Coated Pozzolana and Biogenic Green Rust to Purify Waste Water
440 Containing Phosphate and Nitrate, *Curr. Inorg. Chem* 6, 100-118.

441 [20] Tsuji, H., Fujii, S., 2014. Phosphate recovery by generating hydroxyapatite via reaction of calcium
442 eluted from layered double hydroxides, *Appl. Clay Sci.* 99, 261-265.

443 [21] Vohla, C., Kõiv, M., Bavor, H. J., Chazarenc, F., Mander, Ü., 2011. Filter materials for phosphorus
444 removal from wastewater in treatment wetlands—A review, *Ecol. Eng.* 37, 70-89.

445

446 **Figure captions**

447 **Figure 1:** Evolution of soluble Ca^{2+} and Fe^{3+} concentrations in the supernatant during the interaction
448 of Ca-Fe LDH with P-free demineralized water.

449 **Figure 2:** Evolution of the XRD patterns (a and b) and Raman spectra (c and d) during the interaction
450 of Ca-Fe LDH with P-free demineralized water. (a) and (c) Pristine Ca-Fe LDH materials; (b) and (d) after
451 contact with P-free demineralised water during 24 hours.

452 **Figure 3:** (a) Evolution the PO_4 removal capacity of Ca-Fe LDH as a function of time for different initial
453 phosphate concentrations. (b) Evolution of the maximal removal capacity as a function of the initial
454 phosphate concentration.

455 **Figure 4:** (a) Evolution the XRD patterns for Ca-Fe LDH after contact with PO_4 for different initial
456 phosphate concentrations. (a) Pristine Ca-Fe LDH materials, (b) $[\text{PO}_4]_0 = 20 \text{ mg L}^{-1}$, (c) $[\text{PO}_4]_0 = 100 \text{ mg}$
457 L^{-1} , (d) $[\text{PO}_4]_0 = 200 \text{ mg L}^{-1}$, (e) $[\text{PO}_4]_0 = 300 \text{ mg L}^{-1}$, (f) $[\text{PO}_4]_0 = 400 \text{ mg L}^{-1}$, (g) $[\text{PO}_4]_0 = 500 \text{ mg L}^{-1}$,
458 (h) $[\text{PO}_4]_0 = 600 \text{ mg L}^{-1}$.

459 **Figure 5:** (a) Evolution the XRD patterns for Ca-Fe LDH after contact with PO_4 solution ($[\text{PO}_4]_0 = 600 \text{ mg}$
460 L^{-1}) for different contact times.

461 **Figure 6:** Ions concentrations release from Ca-Fe LDH during the removal process at initial PO_4
462 concentrations from 20 to 1000 mg L^{-1} (0.21 to 10.35 mmol L^{-1}). The samples were taken after 48 hours
463 of reaction.

464 **Figure 7:** TEM images of the transformation products obtained after the interaction of the Ca-Fe LDH
465 with a PO_4 solution ($[\text{PO}_4]_0 = 20 \text{ mg L}^{-1}$).

466 **Figure 8:** Mössbauer spectra of the transformation products obtained after the interaction of the Ca-
467 Fe LDH with a PO_4 solution ($[\text{PO}_4]_0 = 20 \text{ mg L}^{-1}$). The spectra were recorded at a temperature of 77 K
468 (a), 35 K (b) and 14 K (c).

469 **Figure 9:** Evolution of the relative phosphate concentration C / C_0 as a function of V / V_p , where C
470 represents the phosphate concentration in the outflow of the column, C_0 the phosphate concentration
471 in the inflow of the column, V the volume of PO_4 solution introduced in the column and V_p the porous
472 volume of the column. The evolution of the pH during this experiment is also represented.

473 **Figure 10:** Schematic description of the interaction of Ca-Fe LDH in interaction $\text{PO}_{4\text{aq}}$ species as a
474 function of the initial phosphate concentration: (a) $[\text{PO}_4]_0 \leq 100 \text{ mg L}^{-1}$ and (b) $[\text{PO}_4]_0 > 100 \text{ mg L}^{-1}$. HA
475 is hydroxyapatite.

476

477

478

479

480 **Table captions**

481 **Table 1** : Maximal phosphate removal capacity measured by adsorption isotherms for various calcium
482 containing LDH. If available, the values of the initial PO₄ concentration, the LDH dose and the pH of the
483 isotherm experiments are also reported.

484

485 **Table 2**: Chemical analysis by EDX of the products of transformation of Ca-Fe LDH in contact with an
486 initial PO₄ concentration of 20 mg L⁻¹. Three different regions of the sample were analysed.

487 **Table 3** : Hyperfine parameters of the Mössbauer spectra (Fig. 8) measured after contact of a Ca-Fe
488 LDH with a 20 mg L⁻¹ phosphate solution.

489

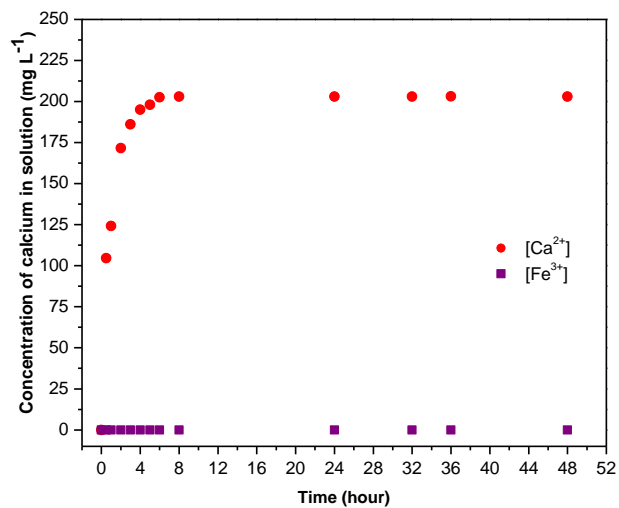
490

491

Figure 1

492

493



497

498

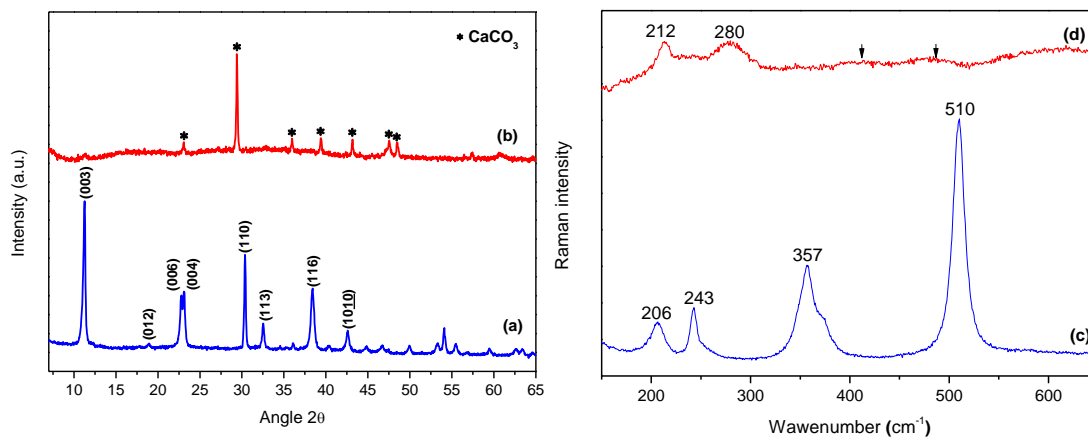
499

500

Figure 2

501

502



503

504

505

506

507

508

509

510

Figure 3

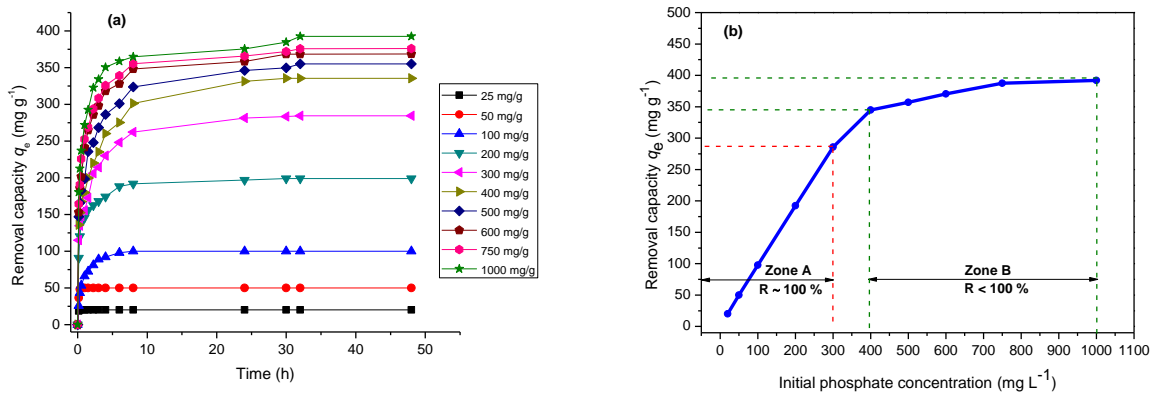
511

512

513

514

515



516

517

Figure 4

518

519

520

521

522

523

524

525

526

527

528

529

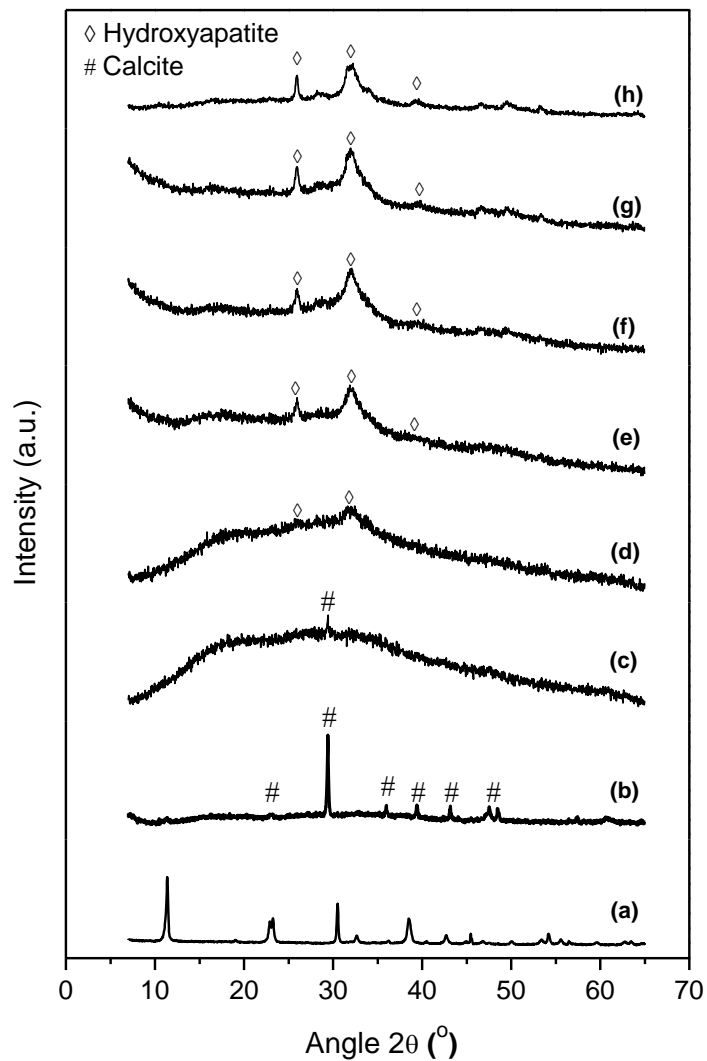
530

531

532

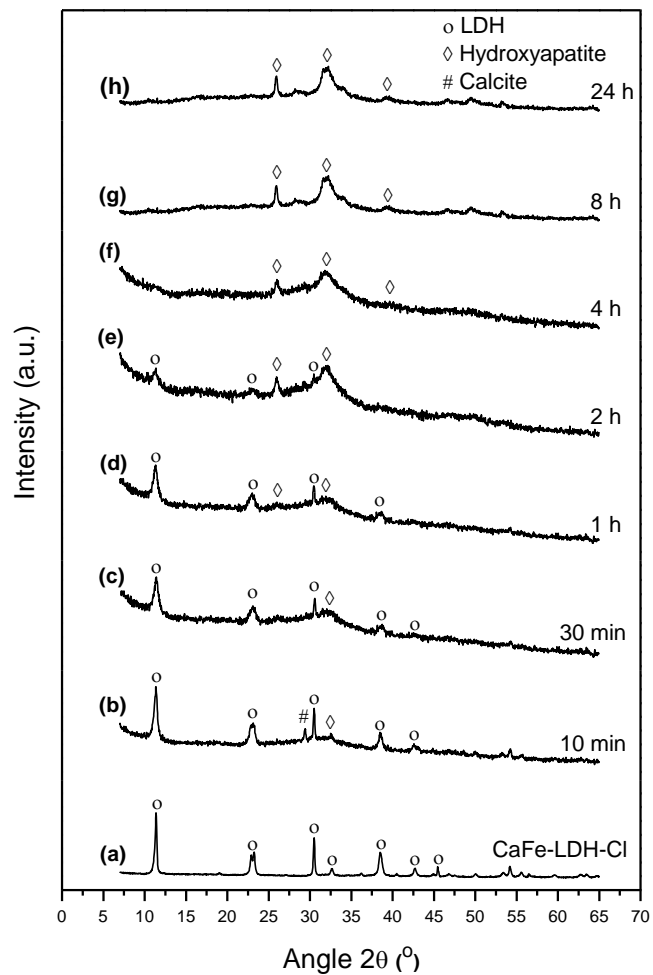
533

534



535
536
537
538
539
540
541
542
543
544
545
546
547
548
549
550
551
552
553
554
555
556
557
558
559
560
561

Figure 5



562

563

Figure 6

564

565

566

567

568

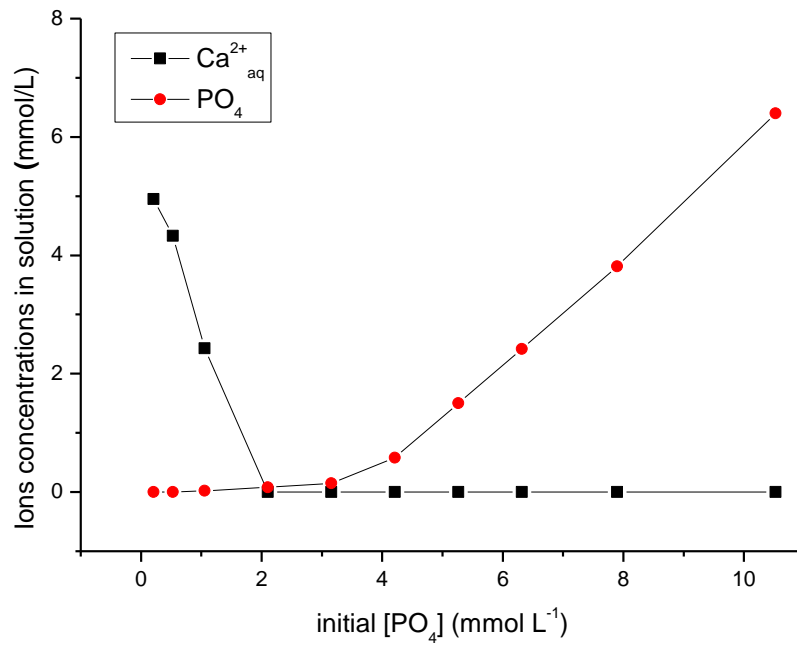
569

570

571

572

573



574

575

576

577

Figure 7

578

579

580

581

582

583

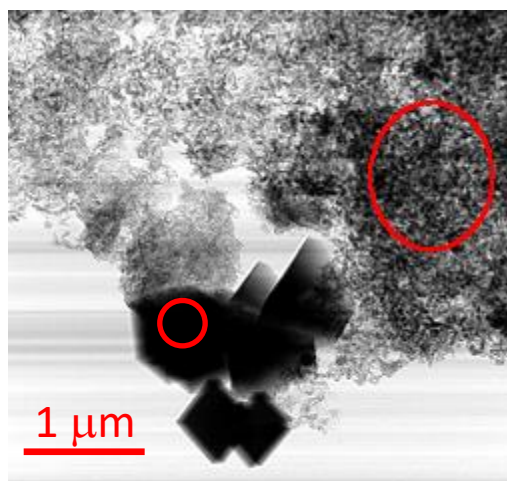
584

585

586

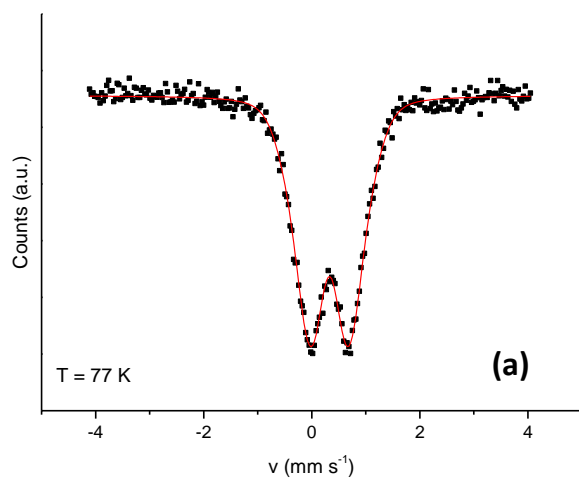
587

588



589

Figure 8



590

591

592

593

594

595

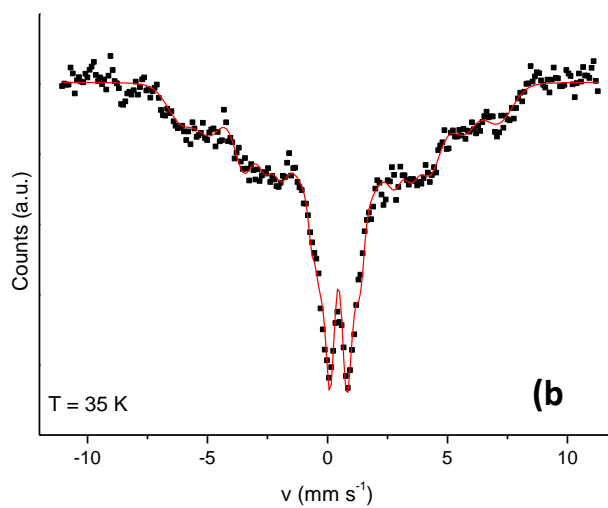
596

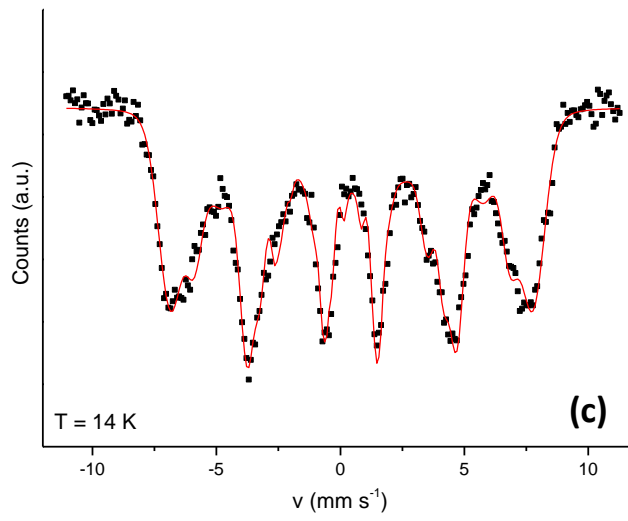
597

598

599

600





601

602

603

Figure 9

604

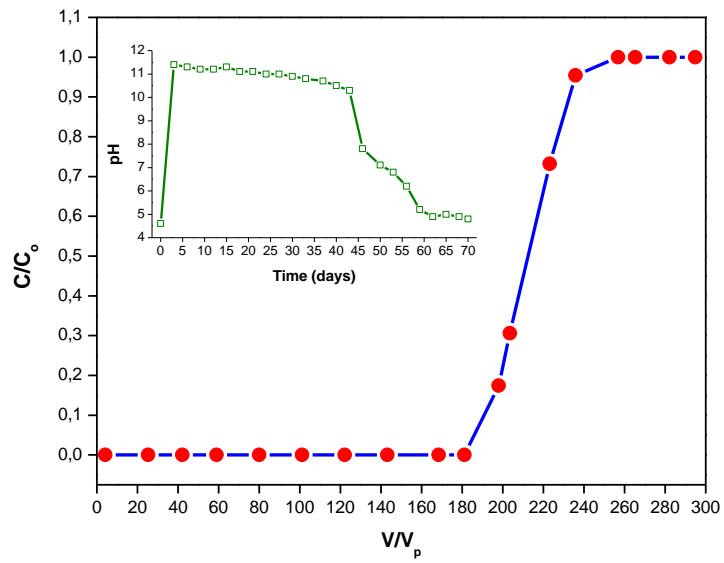
605

606

607

608

609



610

611

612

613

614

615

616

617

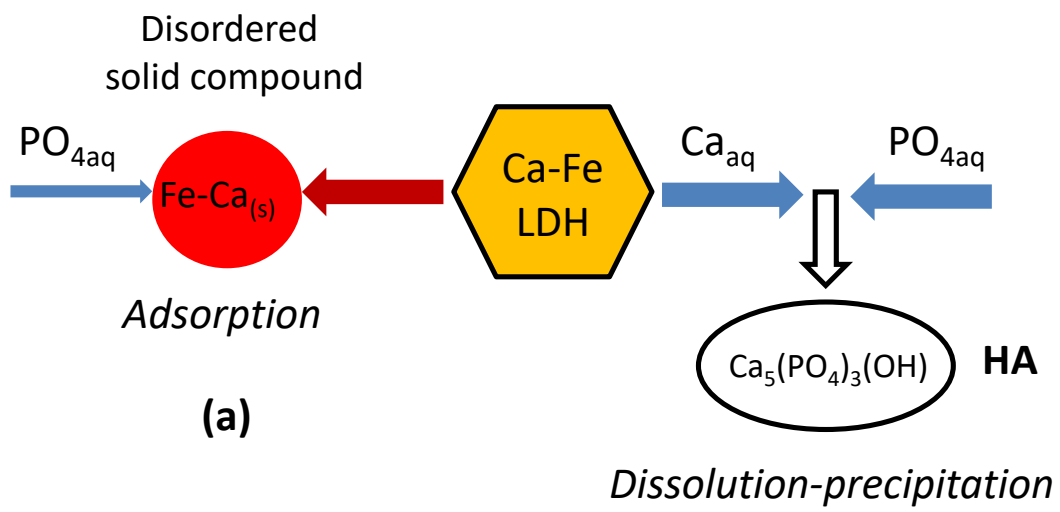
618

619

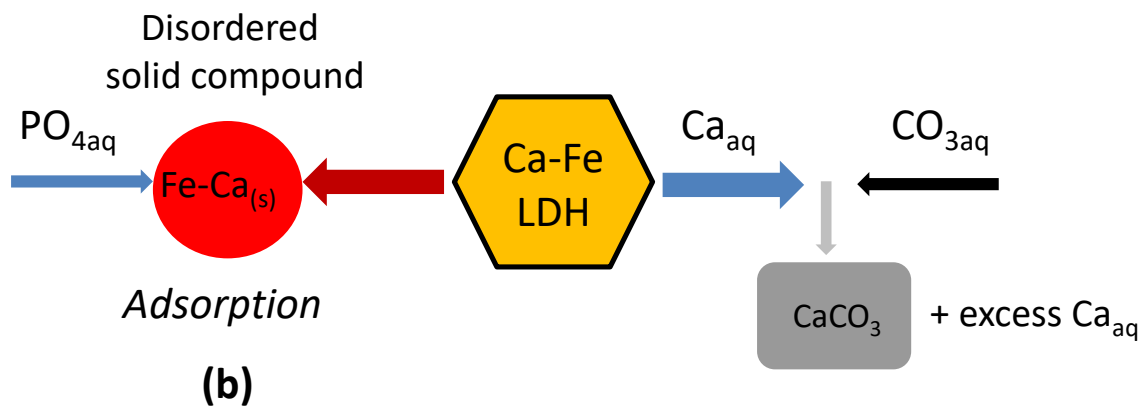
620

621

Figure 10



(a)



(b)

622

623

624

625

626

627

628

629

630

631

632

633
634
635

Table 1

HDL type	$q_e^{(Max)}$ (mg P-PO ₄ g ⁻¹) (*)	$q_e^{(Max)}$ (mmol PO ₄ g ⁻¹)	Initial [PO ₄] (mg L ⁻¹)	LDH dose (g L ⁻¹)	pH	Ref.
Ca-Al-Cl	179	5.8	30-5400	2	4-7	Jia et al., 2016
Ca-Al-Cl	132	4.2	100-500	1	7-9	Qian et al., 2012
Ca-Al-Cl (synthesized from gastropod shell)	69	2.2	25-300	2	(**)	Oladoja et al., 2014
Ca-Al-NO ₃	64	2	50-1000	10	8.1	Bekele et al., 2019)
Ca-Al-NO ₃	66	2.15	~1- ~30	0.3	7	Ashekuzzaman et al., 2014
Ca-Mg-Al-NO ₃	71	2.3	~1- ~30	0.3	7	Ashekuzzaman et al., 2014
Ca-Fe-NO ₃	46	1.5	~1- ~30	0.3	7	Ashekuzzaman et al., 2014
Ca-Fe-Cl	~ 90	~2.9	60-300	0.4	(**)	Tsuji and Fujii, 2014
Ca-Fe-Cl	130	4.2	20-2000	1	7	This work

636 (*) The values reported for $q_e^{(Max)}$ are those corresponding to data obtained by using the fitting of the
637 isotherm experiments (**) The pH values of the isotherm experiments were not provided.

638
639
640
641

642

643

644

Table 2

645

Region	Spot	O (at.%)	P (at.%)	Ca (at.%)	Fe (at.%)
1	A	61.1	5.6	22.4	10.9
	B	49.0	10.6	24.1	16.3
	C	59.6	-	40.4	-
2	D	56.8	5.8	24	13.4
	E	68.1	3.2	9	19.7
	F	59.9	-	40.1	-
3	G	61.6	5.7	22.5	10.2
	H	63.8	4.9	12.2	19.1

646

647

648

649

650

651

652

653

654

655

656

657

658

659

660

Table 3

661

Temp. (K)	Fig. Spectrum	Component	δ (mm s ⁻¹)	Δ or ε (mm s ⁻¹)	H (kOe)	RA (%)
77 K	Fig 8a	D ₁	0.44	0.84	-	100
35 K	Fig 8b	D ₁	0.45	0.71	-	13
		D ₂	0.55	3.2	-	46
		S ₁	0.42	0.02	256	10
		S ₂	0.46	0.06	408	16
		S ₃	0.43	-0.02	328	15
14 K	Fig 8c	D ₁	0.76	1.99	-	10
		S ₁	0.49	0.003	270	29
		S ₂	-2.8	-0.46	133	3
		S ₃	0.45	0	453	40
		S ₄	0.46	0	394	18

662

663 δ : Isomer shift, Δ or ε : Quadrupole shift or quadrupole splitting, H : Hyperfine field, RA : Relative area of the
664 component.

665

666

667

668

669

670